Available online at www.sciencedirect.com
ScienceDirect
Trans. Nonferrous Met. Soc. China 28(2018) 839−847
Transactions of Nonferrous Metals Society of China
www.tnmsc.cn

Influence of different solution methods on microstructure, precipitation behavior and mechanical properties of Al−Mg−Si alloy

Guan-jun GAO[1], Chen HE[1], Yong LI[1], Jia-dong LI[1], Zhao-dong WANG[1], R. D. K. MISRA[2]

1. State Key Laboratory of Rolling and Automation, Northeastern University, Shenyang 110819, China;
2. Laboratory for Excellence in Advanced Steel Research, Department of Metallurgical, Materials and Biomedical Engineering, University of Texas at El Paso, El Paso, TX 79968, USA

Received 27 December 2016; accepted 24 April 2017

Abstract: The effects of different solution methods on microstructure, mechanical properties and precipitation behavior of Al−Mg−Si alloy were investigated by scanning electron microscope, transmission electron microscope, tensile test, and differential scanning calorimetry. The results revealed that the recrystallized grains of the alloy after the solution treatment with hot air became smaller and more uniform, compared with solution treatment with electrical resistance. The texture of the alloy after two solution treatment methods was different. More rotated cube components were formed through solution treatment with electrical resistance, which was better for improving the drawability of the alloy. The strength of the alloy under the solution treatment with hot air was higher before stamping, because of the small uniform grains and many clusters in the matrix. The alloy solution treated with hot air also possessed good bake hardenability, because the transformation occurred on more clusters in the matrix.

Key words: Al−Mg−Si alloy; solution method; recrystallization grain; texture; mechanical property; precipitation activation energy

1 Introduction

In recent years, the heat-treatable Al−Mg−Si alloys have played an important role in automotive body sheet materials. The first step aging after solution treatment is beneficial to stamping and maintaining resistance to natural aging during transportation [1]. The alloys achieve quick-bake hardening (BH) response after the second step aging. Extensive studies have been reported on the two-step aging process [2−5]. However, solution treatment before artificial aging influences the microstructure, especially grain size and texture, and further influences formability and final properties of alloys [6,7]. There are many different heating methods during solution treatment, such as electrical resistance, hot air and salt bath. Thus, it is important to choose an appropriate solution method for automotive body sheets in industrial production.

The effects of different solution heat treatment rates on the microstructure and texture were studied [7,8]. LIU and MORRIS [7] observed coarse and elongated recrystallized grains and relatively strong P type texture formed on slow annealing. On the contrary, the recrystallization texture contained weak cube component during rapid annealing treatment and the size of grains was governed by the annealing temperature in AA3105 aluminium alloy. WANG et al [9] observed weaker mechanical property anisotropy and more uniform equiaxed grains formed with rapid heating rate. The equiaxed grains are the main recrystallization microstructure in the case of rapid heating rate, while the elongated grain appears in the case of slow heating rate based on the study of Al−Mg−Si alloy with different heating rates. However, the above findings did not involve the influence of different solution methods including heating rate and uniformity. Few works have been studied about the influence of different solution methods on Al−Mg−Si alloy. It is still unclear whether the solution methods will affect the precipitation behavior and nano- precipitates.

Two solution methods were adopted in this study.

Foundation item: Project (2016YFB0300605) supported by the National Key Research and Development Program of China; Project (51234002) supported by the National Natural Science Foundation of China, Project (L2013113) supported by the Liaoning Province Science and Technology, China; Project (N140703002) supported by the Fundamental Research Funds for the Central Universities, China
Corresponding author: Yong LI; Tel: +86-24-83681803; Fax: +86-24-23906472; E-mail: liyong@ral.neu.edu.cn
DOI: 10.1016/S1003-6326(18)64717-X

The following experimental conditions for the two-step aging process are same to eliminate the factors introduced by the differences in heating treatment conditions. The goal of this study is to investigate the effect of two solution methods on microstructure evolution, precipitation behavior and mechanical properties of Al−Mg−Si alloy.

2 Experimental

A commercial Al−Mg−Si alloy cold rolled to 1 mm in thickness was prepared for this study. Homogenization and hot rolling process were carried out prior to cold rolling. The homogenized alloy was heated at 540 °C for 25 h and then air-cooled to room temperature. The alloy sheet was hot rolled to 5 mm in thickness before cold rolling. The chemical composition of the sheet was measured by inductively coupled plasma optical emission spectroscopy, and determined to be Al−0.55Mg−1.10Si−0.14Fe−0.10Cr (mass fraction, %).

The alloy was divided into two parts for different solution treatment methods. Sheet A was heated in air-circulation oven, and sheet B was heated in electrical resistance oven. The heating curves of solution treatment are shown in Fig. 1. Sheets with different heating methods were solution-treated at 560 °C for 30 min, water-quenched to room temperature (RT), and then immediately pre-aged at 160 °C for 8 min in an air-circulation oven, air-cooled to RT, finally placed at RT for two weeks (T4P). 2% tensile deformation was applied to simulating the stamping process. The bake hardening was heat treated at 175 °C for 30 min, in an air-circulation oven and air-cooled to RT. Figure 2 shows the processing route of heat treatment.

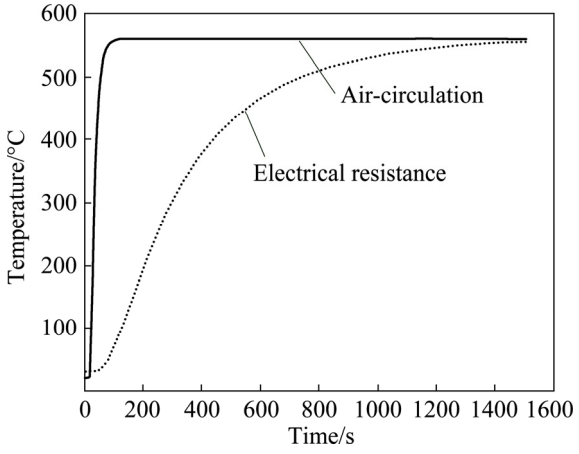

Fig. 1 Heating curves of alloy sheets solution-treated in air-circulation oven and electrical resistance oven

The recrystallization microstructure and texture of longitudinal sections of sheet (T4P) were characterized with a field emission scanning electron microscope (ZEISS ULTRA 55), equipped with an electron backscattered diffraction (EBSD). Precipitates in the matrix were observed using a Tecnai G2 F20 transmission electron microscopy (TEM) operated at 200 kV. Specimens were prepared with a TenuPol-5 jet-polisher. The electrolyte consisted of HNO_3 and CH_3OH (3:7), and the temperature of the electrolyte was kept between −20 and −25 °C. Tensile tests were performed in accordance with the China Standard (GB/T 228−2002) using a 10 t INSTRON 4206 type testing machine. The properties of sheets in three directions of 0°, 45° and 90° with respect to the rolling direction were tested before 2% tensile deformation (T4P state), including yield strength ($R_{p0.2}$), ultimate tensile strength (R_m) and plastic strain ratio (r) values. The sheets in the 0^o direction after bake hardening were also investigated. The strain rate was 3 mm/min. Differential scanning calorimetry (DSC) was carried out with Q100 differential scanning calorimeter. Samples for DSC analyses were 0.5 mm in thickness and 5 mm in diameter, and were cleaned with ultrasonic wave pool. They were obtained after 2% tensile deformation. The mass of each sample was about 20 mg. Empty pure aluminium crucibles were used as container and reference material. The samples for DSC testing were heated from RT to 400 °C at 10 °C/min under an argon atmosphere.

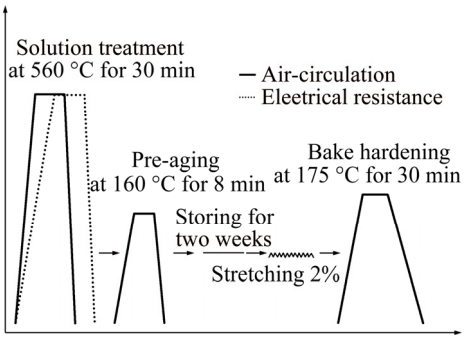

Fig. 2 Heating treatment process for aluminum alloy sheet

3 Results and discussion

3.1 Recrystallization microstructure

To study the differences in recrystallization microstructure between sheets A and B, EBSD analysis of samples with T4P state was performed. Figure 3 shows the IPF maps and volume fraction diagram of grain size for sheets A and B, respectively. Obviously, the recrystallized equiaxed grains of sheet A were more uniform than that of sheet B, because of the presence of very large grains, as shown in Fig. 3(b). According to the results of statistical calculation, the average grain size of sheet A (21.58 μm) was smaller than that of sheet B (25.64 μm). The uniformity and size of recrystallized grains for sheets A and B are related to different solution methods.

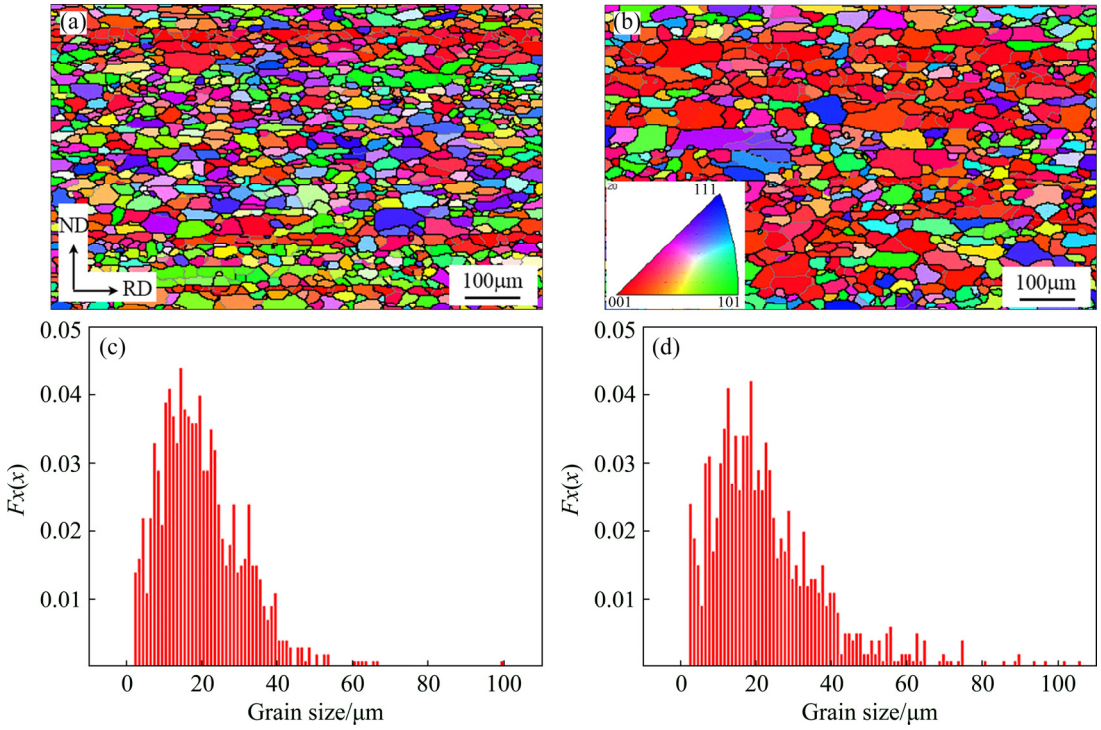

Fig. 3 IPF maps (a, b) and volume fractions (c, d) of sheets with T4P state: (a, c) Solution treatment with hot air; (b, d) Solution treatment with electrical resistance (Recrystallization grain size distribution function of sheets)

The main difference in the solution methods between sheets A and B is heating rate and uniformity. The heating rate of solution treatment for sheet A was larger than that of sheet B as shown in Fig. 1. Samples heated in air-circulation oven were more uniform during solution treatment. This led to the difference in microstructure between sheets A and B. Faster heating means that external condition can provide higher driving force for recrystallization. Nucleation is promoted when the driving force is high. In addition, uniformity in heating also affects the recrystallization microstructure. Nucleus of recrystallized grains distribute unevenly in the matrix in the case of local overheating, and individual grains become coarse after solution treatment [10]. Therefore, the recrystallized grain of sheet A was smaller and more homogeneous than that of sheet B, as shown in Fig. 3.

3.2 Texture and drawability

Bright-field TEM images for sheets A and B after bake hardening are shown in Fig. 4. Since new dispersed particles would not form by heating below 200 °C for short time (e.g., pre-aging and bake hardening). Thus, samples after bake hardening can be used for TEM observations. The average size of these dispersed sphere or rod-shaped particles observed in sheet A was 300 nm. There were also some coarse particles over 1 μm embedded in the matrix. EDS analysis indicated that these single coarse particles were AlMgSiCr intermetallic compounds containing Cr element, as shown in Figs. 4(a) and (b). On the contrary, only spherical or rod-shaped particles were observed in sheet B, there was no presence of coarse particles. The compositions of these dispersed particles in sheet A or B matrix, were composed of Al, Mn, Fe, Cr and Si elements, as seen in Figs. 4(c) and (d). The existence of these particles had an effect on the recrystallization texture of the alloy.

Figure 5 shows the ODFs of sheets with T4P state. The difference in recrystallization texture between sheets A and B can be easily observed. Sheet A was composed of typical $cube_{RD}$ orientation, accompanied by P $\{011\}\langle 122\rangle$ components. But the intensity of dominant recrystallization texture $cube_{RD}$ orientation was only 5.2. On the contrary, the main texture component of sheet B was $cube_{ND}$ orientation, accompanied by a small amount of P $\{011\}\langle 122\rangle$ and Brass $\{011\}\langle 211\rangle$ orientation. However, compared with sheet A, the intensity of cube orientation was 9.4 for sheet B. The main texture volume fractions for sheets A and B were 10.2% and 19.8%, respectively. The details of typical recrystallization texture components are summarized in Table 1.

Some researchers [9,11,12] indicated that if there are a certain amount of coarse particles (greater than 1 μm) in the matrix, it resulted in particle stimulated nucleation (PSN) response during solution treatment for

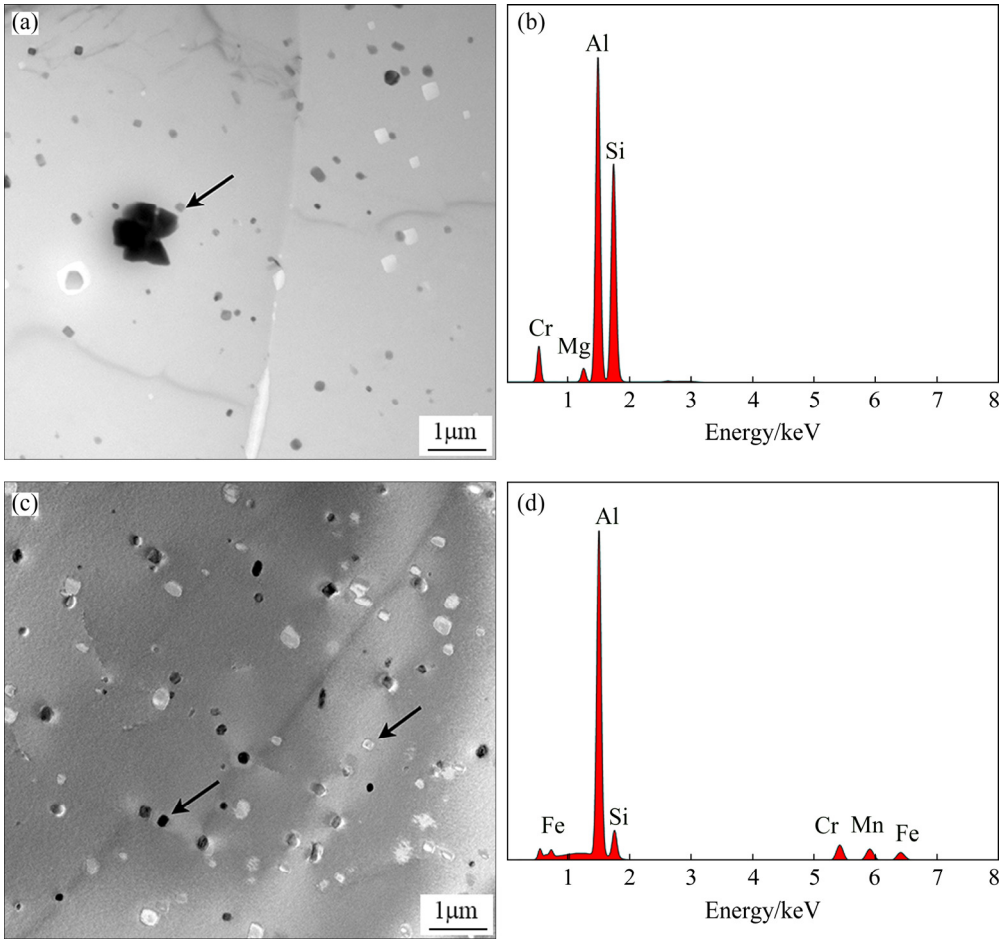

Fig. 4 Bright-field TEM images (a, c) and corresponding EDS analyses (b, d) of coarse particles in sheets: (a, b) Solution treatment with hot air; (c, d) Solution treatment with electrical resistance

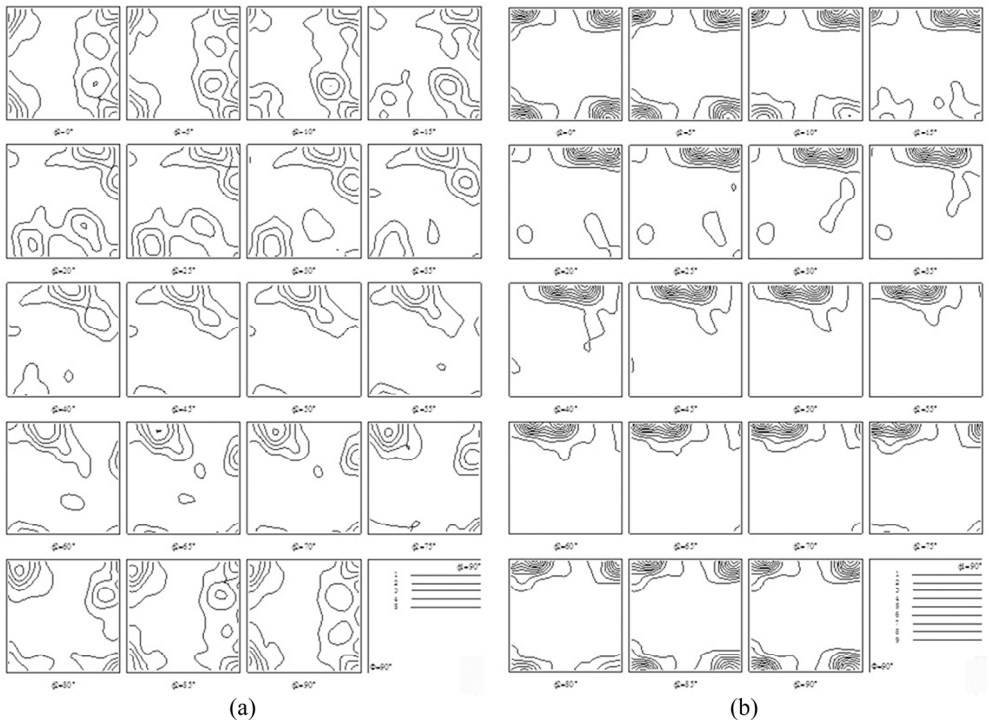

Fig. 5 Recrystallization texture of sheets with T4P state: (a) Solution treatment with hot air; (b) Solution treatment with electrical resistance

Table 1 Intensity and volume fraction of typical recrystallization texture components for sheets solution treated with hot air and electrical resistance obtained from ODFs

Sheet	Component	Intensity	Volume fraction/%
A	$Cube_{RD}$	5.2	10.2
	P {011}⟨122⟩	1.8	7.5
B	$Cube_{ND}$	9.4	19.8
	P {011}⟨122⟩	0.6	3.3
	Brass {011}⟨211⟩	0.5	3.7

aluminium alloys. A number of recrystallization nuclei form around these coarse particles. The subsequent recrystallization texture components mainly contained rotated cube and P types. In our study, coarse particles were observed (Fig. 4(a)) in sheet A matrix. The texture components of sheet A were $cube_{RD}$ and a small P orientation with PSN mechanism, as shown in Fig. 5(a). On the contrary, only some micron-sized dispersed particles formed during recrystallization in sheet B at slow heating rate (Fig. 4(c)). The appearance of these fine particles effectively prevents recrystallized grains from rotating along ND and RD orientations. Thus, the texture component is mainly $cube_{ND}$ orientation (Fig. 5(b)).

Figure 6 shows that r values with T4P state were different in three directions. The r value in the 45° direction was lower than the other two directions. In addition, the average r value of sheet A was 0.62, lower than 0.72 of sheet B with T4P state. Generally, the value of r reflects deep drawability of sheets, and a high r value is beneficial for stamping. Texture components have a great effect on the r value. It is reported that rotated cube and P texture are favorable to improve the deep drawability [13]. The stimulated r value corresponding to cube component is 0.5, and that of P component is 2.8 [9]. LIU et al [14] indicated that $cube_{ND}$ texture is more obvious to increase r value than cube texture, the corresponding r value is greater than 0.5. In this study, although the volume fraction of P component for sheet A was higher than sheet B and recrystallized grains were smaller and more uniform, with high volume fraction of $cube_{ND}$ component for sheet B, the effect in increasing r value was more remarkable than sheet A.

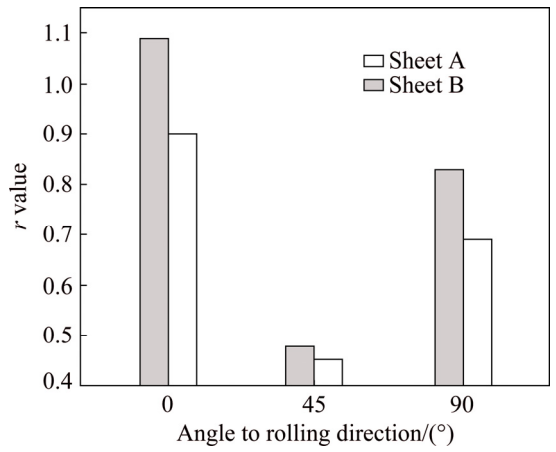

Fig. 6 r value of sheets solution treated with hot air and electrical resistance with T4P state in three directions

3.3 Mechanical properties and precipitation behavior

Strength increment in automotive body sheets is needed after bake hardening in order to meet the dent resistance. Figure 7 shows the stress−strain curves of sheets A, B with T4P and BH treatment. For individual sheet A or B, the strengths in three different directions were almost the same. The average yield strength of sheet A was higher than that of sheet B. Strength increment in the 0° direction for sheet A was higher than that for sheet B (104 and 90 MPa respectively) after bake hardening. The detailed mechanical properties of sheets A and B are shown in Table 2.

Apart from the intermetallic compounds, some needle-shaped precipitates were observed in the Al

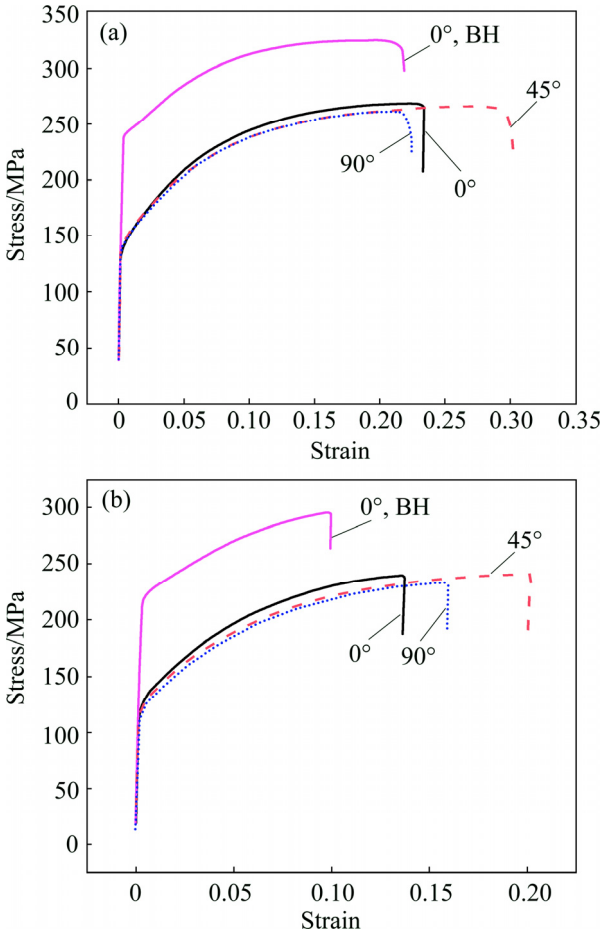

Fig. 7 Stress−strain curves of sheets with T4P and BH treated in three directions of 0°, 45° and 90° with respect to rolling direction: (a) Solution treatment with hot air; (b) Solution treatment with electrical resistance

Table 2 Mechanical properties of sheets solution treated with hot air and electrical resistance with T4P in three directions of 0°, 45° and 90° with respect to rolling direction

Sheet	Direction/(°)	$R_{p0.2}$/MPa	R_m/MPa
A	0	139	270
	45	140	265
	90	139	260
	0 (BH)	243	325
B	0	128	240
	45	126	240
	90	125	235
	0 (BH)	218	295

matrix, which formed during bake hardening [1,15]. These precipitates appeared in the matrix during bake hardening were the main reason for the strength increment [16,17]. Figure 8 shows HRTEM images of the precipitate and corresponding fast Fourier transform (FFT) image. The images were projected along [001] and [110] axes of Al matrix, respectively. According to the conclusion of calibration, the unit cell of these precipitates was C-centered monoclinic crystal structure with a=1.52 nm, c=0.67 nm and β=105.25°. The orientation relationship between β'' precipitates and Al matrix can thus be expressed as: $(010)_{\beta''}$// $(00\bar{1})_{Al}$, $[001]_{\beta''}$//$[130]_{Al}$, and $[100]_{\beta''}$//$[3\bar{2}0]_{Al}$. The misfit degree was 3.8% along a axis between the unit cell and matrix, 5.3% along c axis, and b axis of precipitate was completely coherent with $[001]_{Al}$ [15,18−20]. These precipitates embedded in the matrix are identified as β'' phase, which is the major hardening phase [21]. HRTEM image projected along $[110]_{Al}$ axis is shown in Fig. 8(c). The length of β'' precipitate was ~15 nm and four atom layers in thickness. The plane of precipitate was parallel to $(\bar{1}1\bar{1})_{Al}$. Needle-shaped β'' precipitates were more projected along $[110]_{Al}$ axis than along $[001]_{Al}$ axis.

To study the precipitation behavior during bake hardening and further explain the different mechanical properties of sheets A and B, DSC was performed at a heating rate of 10 °C/min. Figure 9 shows the DSC thermograms obtained for sheets A and B. The response to DSC heating of these samples agrees with the

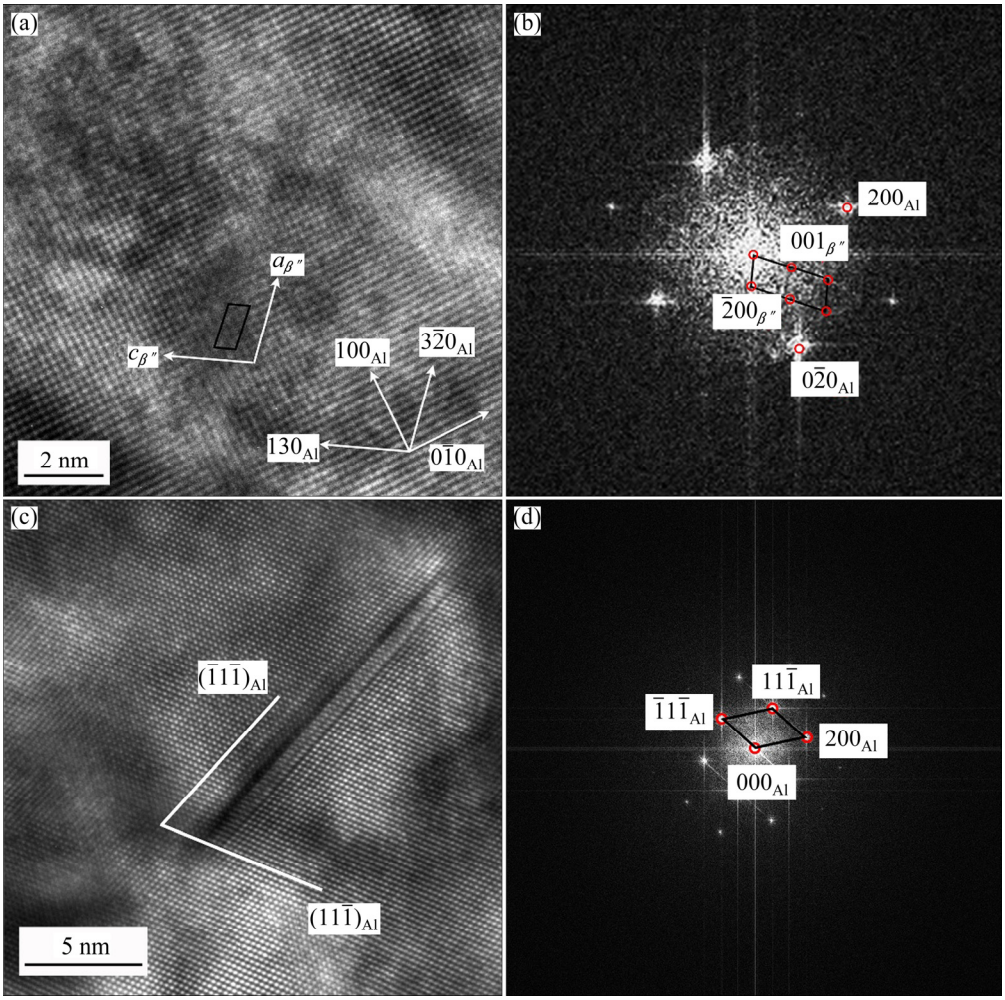

Fig. 8 HRTEM images of needle-shaped precipitate: (a) Projected along $[001]_{Al}$ axis; (b) FFT pattern of (a); (c) Projected along $[110]_{Al}$ axis; (d) FFT pattern of (c)

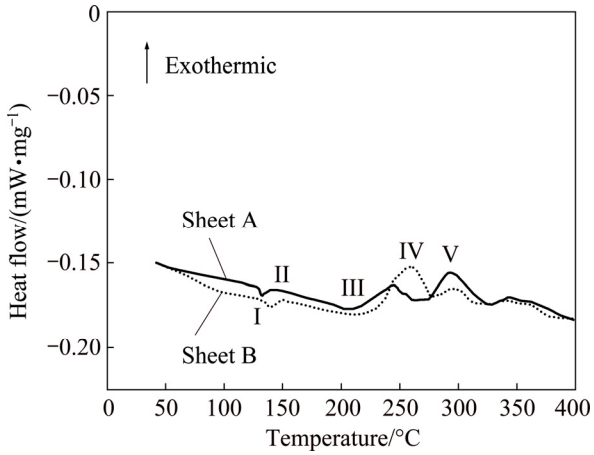

Fig. 9 DSC thermograms for sheets solution treated with hot air and electrical resistance with T4P state samples obtained at heating rate of 10 °C/min

well-established precipitation sequence of Al−Mg−Si alloys: supersaturated solid solution→clusters/zones→ $\beta''\rightarrow\beta'\rightarrow\beta$ [19].There were several endothermic and exothermic peaks in DSC curves from RT to 400 °C. The endothermic peak I may be caused by initial β'' formed during pre-aging treatment, re-dissolved into Al matrix [22]. The neighboring small exothermic peak II at ~135 °C is supposed to be the result of formation of GP zones. The endothermic peak III associated with the redissolution of GP zones formed. Peaks IV and V of sheets A and B are mainly related to the appearance of β'' and β' precipitates, respectively [23−26]. From the thermograms of sheets A and B, the temperature of exothermic peaks for sheet A was all lower than that for sheet B.

According to Johnson−Mehl−Avrami equations (1) and (2) [27−29], the activation energy of given precipitates with Q, can be obtained from the slope of the straight line fitted.

$$Y=1-\exp(-kt^n) \quad (1)$$

$$k=k_0\exp[-Q/(RT)] \quad (2)$$

Since automotive body sheets were applied in under-aged condition, only activation energies of GP zone and β'' precipitates were calculated in the present work. Figure 10 shows the linear fit to data plots according to Johnson-Mehl-Avrami equation for peaks II and IV. Since overlapping effects and an uncertain baseline construction for the thermograms of sheets A and B, deviations for the calculated value of activation energy may be present. As shown in Fig. 10(a), the obtained activation energy of GP zone for sheet A was 63 kJ/mol, while 66 kJ/mol for sheet B. Figure 10(b) shows that the values of β'' precipitate for sheets A and B were 124 and 118 kJ/mol, respectively. All plots had a good linear correlation, and there were no obvious errors

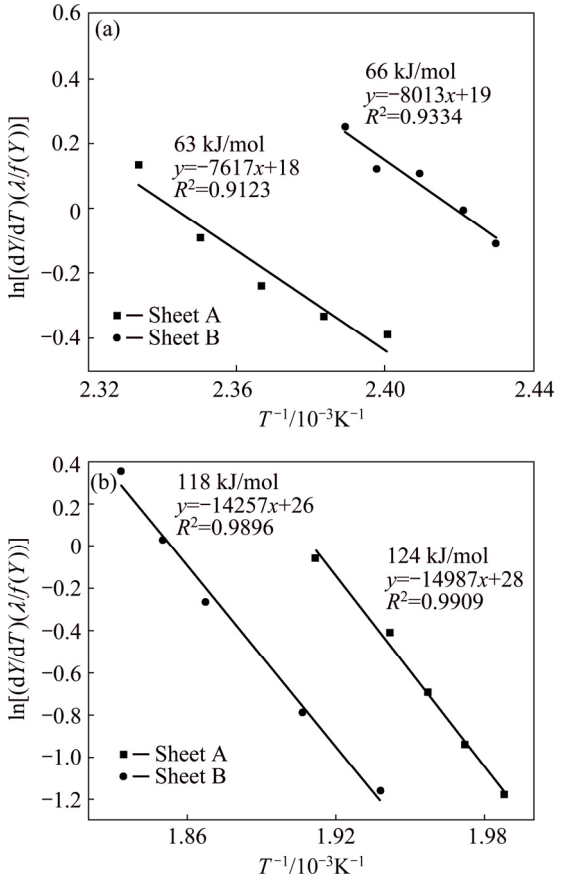

Fig. 10 Linear fit to data plots according to Johnson−Mehl−Avrami equation for GP zone (a) and β'' precipitate (b)

among the calculated values according to the previous researches [10,24,29,30].

Mechanical properties of sheets are influenced by microstructure and particles. The smaller and more uniform recrystallized grains contribute to the high strength of sheet A with T4P state (Fig. 3(a) and Table 2). Moreover, soluble phases dissolved in the matrix after solution treatment, despite the influence of insoluble phases, the main particle is nano-precipitate $Mg_2Si_2Al_7$ [15], which forms at low temperature and remains stable at RT. Sheet A possesses higher free energy because of the contribution of smaller recrystallized grains. The volume fraction of $Mg_2Si_2Al_7$ phases in sheet A was larger than that of sheet B for the identical heat treatment. Therefore, the strength of sheet A with T4P state was higher compared with that of sheet B. Actually the value of strength is influenced by the interaction of all the above factors. Stable $Mg_2Si_2Al_7$ phases at RT rapidly transform into $Mg_{2+x}Si_{2+y}Al_{7-x-y}$ during bake hardening, a small amount of β'' precipitates appear concurrently [15]. The dent resistance of sheets is improved. These nano-precipitates are the dominant strengthening phase of sheets in application. Since activation energies of GP zone and β'' phase for sheets A and B are almost the same. The sheet A with higher free

energy forms more strengthening precipitates under identical heat treatment condition during bake hardening [31,32]. Therefore, the increment in the strength of sheet A is higher than that of sheet B.

4 Conclusions

1) The recrystallized grains of sheet with air-circulation method and electrical resistance solution method led to equiaxed grains. Compared with the electrical resistance solution method, the grains of sheet solution treated in air-circulation oven were smaller and more uniform.

2) The main textures of sheet with the air-circulation solution method were $cube_{RD}$ and P components by PSN mechanism, while texture of sheet with the other solution method was $cube_{ND}$, accompanied by a small amount of P and Brass components. Deep drawability was influenced by texture component, and high volume fraction of $cube_{ND}$ component for sheet with the electrical resistance solution method, was more favorable with increasing r value.

3) The strength of sheet with T4P state solution treated in air-circulation and electrical resistance oven possessed relatively low value, but was higher for the former method, which influenced recrystallized grains and nano-precipitates. The transformation of $Mg_2Si_2Al_7$ phases in the sheet with the air-circulation solution method was larger than that with the electrical resistance solution method during bake hardening. Accordingly, the increment of strength for the sheet with the former method was higher than that of the latter solution method.

References

[1] PASHLEY D W, JACOBS M H, VIETZ J T. The basic processes affecting two-step ageing in an Al−Mg−Si alloy [J]. Philosophical Magazine, 1967, 16(139): 51−76.

[2] POGATSCHER S, ANTREKOWITSCH H, LEITNER H, SOLOGUBENKO A S, UGGOWITZER P J. Influence of the thermal route on the peak-aged microstructures in an Al−Mg−Si aluminum alloy [J]. Scripta Materialia, 2013, 68(2): 158−161.

[3] KIM J H, MARIOARA C D, HOLMESTAD R, KOBAYASHI E, SATO T. Effects of Cu and Ag additions on age-hardening behavior during multi-step aging in Al−Mg−Si alloys [J]. Materials Science & Engineering A, 2013, 560: 154−162.

[4] CHEN Wei, GUAN Ying-ping, WANG Zhen-hua. Hot deformation behavior of high Ti 6061 Al alloy [J]. Transactions of Nonferrous Metals Society of China, 2016, 26(2): 369−377.

[5] HUANG Yuan-chun, YAN Xu-yu, QIU Tao. Microstructure and mechanical properties of cryo-rolled AA6061 Al alloy [J]. Transactions of Nonferrous Metals Society of China, 2016, 26(1): 12−18.

[6] FERRY M, JONES D. High-rate annealing of single-phase and particle-containing aluminium alloys [J]. Scripta Materialia, 1997, 38(2): 177−183.

[7] LIU W C, MORRIS J G. Evolution of recrystallization and recrystallization texture in continuous-cast AA 3015 aluminum alloy [J]. Metallurgical and Materials Transactions A, 2005, 36(10): 2829−2848.

[8] ENGLER O, HIRSCH J. Texture control by thermomechanical processing of AA6xxx Al−Mg−Si sheet alloys for automotive applications—A review [J]. Materials Science & Engineering A, 2002, 336(1−2): 249−262.

[9] WANG Xiao-feng, GUO Ming-xing, CAO Ling-yong, LUO Jin-ru, ZHANG Ji-shan, ZHUANG Lin-zhong. Effect of heating rate on mechanical property, microstructure and texture evolution of Al−Mg−Si−Cu alloy during solution treatment [J]. Materials Science & Engineering A, 2015, 621: 8−17.

[10] VEDANI M, ANGELLA G, BASSANI P, RIPAMONTI D, TUISSI A. DSC analysis of strengthening precipitates in ultrafine Al−Mg−Si alloys [J]. Journal of Thermal Analysis and Calorimetry, 2007, 87(1): 277−284.

[11] PENG Xiang-yang, GUO Ming-xing, WANG Xiao-feng, CUI Li, ZHANG Ji-shan, ZHUANG Lin-zhong. Influence of particles with different sizes on microstructure, texture and mechanical properties of Al−Mg−Si−Cu series alloys [J]. Acta Metallurgica Sinica, 2015, 51(2): 169−177.

[12] ENGLER O, YANG P, KONG X W. On the formation of recrystallization textures in binary Al−1.3%Mn investigated by means of local texture analysis [J]. Acta Materialia, 1996, 44(8): 3349−3369.

[13] WANG Xiao-feng, GUO Ming-xing, ZHANG Yan, XING Hui, LI Yong, LUO Jin-ru, ZHANG Ji-shan, ZHUANG Lin-zhong. The dependence of microstructure, texture evolution and mechanical properties of Al−Mg−Si−Cu alloy sheet on final cold rolling deformation [J]. Journal of Alloys & Compounds, 2015, 657: 906−916.

[14] LIU Y S, KANG S B, KO H S. Texture and plastic anisotropy of Al−Mg−0.3Cu−1.0Zn alloys [J]. Scripta Materialia, 1997, 37(4): 411−417.

[15] CHEN J H, COSTAN E, VAN HUIS M A, XU Q, ZANDBERGEN H W. Atomic pillar-based nanoprecipitates strengthen AlMgSi alloys [J]. Science, 2006, 312(5772): 416−9.

[16] JIA Zhi-hong, DING Li-peng, WENG Yao-yao, WEN Zhang, LIU Qing. Effects of high temperature pre-straining on natural aging and bake hardening response of Al−Mg−Si alloys [J]. Transactions of Nonferrous Metals Society of China, 2016, 26(4): 924−929.

[17] ABDULWAHAB M, MADUGU I A, YARO S A, HASSAN S B, POPOOLA A P I. Effects of multiple-step thermal ageing treatment on the hardness characteristics of A356.0-type Al−Si−Mg alloy [J]. Materials & Design, 2011, 32(3): 1159−1166.

[18] YANG Wen-chao, WANG Ming-pu, ZHANG Rui-rong, ZHANG Qian, SHENG Xiao-fei. The diffraction patterns from β'' precipitates in 12 orientations in Al−Mg−Si alloy [J]. Scripta Materialia, 2010, 62(9): 705−708.

[19] EDWARDS G A, STILLER K, DUNLOP G L, COUPER M J. The precipitation sequence in Al−Mg−Si alloys [J]. Acta Materialia, 1998, 46(11): 3893−3904.

[20] ANDERSEN S J, MARIOARA C D, VISSERS R, FRØSETH A, ZANDBERGEN H W. The structural relation between precipitates in Al−Mg−Si alloys, the Al-matrix and diamond silicon, with emphasis on the trigonal phase U1-$MgAl_2Si_2$ [J]. Materials Science & Engineering A, 2007, 444(1−2): 157−169.

[21] ZANDBERGEN H W, ANDERSEN S J, JANSEN J. Structure determination of Mg_5Si_6 particles in al by dynamic electron diffraction studies [J]. Science, 1997, 277(5330): 1221−1225.

[22] BUHA J, LUMLEY R N, CROSKY A G. Microstructural development and mechanical properties of interrupted aged Al−Mg−Si−Cu alloy [J]. Metallurgical and Materials Transactions A,

2006, 37(10): 3119−3130.
[23] LIU M, ROVEN H J, YU Y, WERENSKIOLD J C. Deformation structures in 6082 aluminium alloy after severe plastic deformation by equal-channel angular pressing [J]. Materials Science & Engineering A, 2008, 483−484(87): 59−63.
[24] POGATSCHER S, ZHANG Z L, UGGOWITZER P J, ANTREKOWITSCH H, LEITNER H, PÖSCHMANN D. Influence of interrupted quenching on artificial aging of Al−Mg−Si alloys [J]. Acta Materialia, 2012, 60(11): 4496−4505.
[25] WEATHERLY G C, PEROVIC A, MUKHOPADHYAY N K, LLOYD D J, PEROVIC D D. The precipitation of the *Q* phase in an AA6111 Alloy [J]. Metallurgical and Materials Transactions A, 2001, 32(2): 213−218.
[26] CHAKRABARTI D J, LAUGHLIN D E. Phase relations and precipitation in Al−Mg−Si alloys with Cu additions [J]. Progress in Materials Science, 2004, 49(3−4): 389−410.
[27] FANG X, SONG M, LI K, DU Y. Precipitation sequence of an aged Al−Mg−Si alloy [J]. Journal of Mining & Metallurgy, 2010, 46(2): 171−180.
[28] GHOSH K S, DAS K, CHATTERJEE U K. Kinetics of solid-state reactions in Al−Li−Cu−Mg−Zr alloys from calorimetric studies [J]. Metallurgical and Materials Transactions A, 2007, 38(9): 1965−1975.
[29] LIU Man-ping, WU Zhen-jie, YANG Rui, WEI Jiang-tao, YU Ying-da, SKARET P C. DSC analyses of static and dynamic precipitation of an Al−Mg−Si−Cu aluminum alloy [J]. Progress in Natural Science, 2015, 25(2): 153−158.
[30] CHOI S W, CHO H S, KANG C S, KUMAI S. Precipitation dependence of thermal properties for Al−Si−Mg−Cu−(Ti) alloy with various heat treatment [J]. Journal of Alloys & Compounds, 2015, 647: 1091−1097.
[31] SERIZAWA A, HIROSAWA S, SATO T. Three-dimensional atom probe characterization of nanoclusters responsible for multistep aging behavior of an Al−Mg−Si alloy [J]. Metallurgical and Materials Transactions A, 2008, 39(2): 243−251.
[32] DU Y, CHANG Y A, HUANG B, GONG W, JIN Z, XU H. Diffusion coefficients of some solutes in fcc and liquid Al: Critical evaluation and correlation [J]. Materials Science & Engineering A, 2003, 363(1−2): 140−151.

不同固溶方式对 Al−Mg−Si 合金组织性能及析出行为的影响

高冠军[1]，贺 晨[1]，李 勇[1]，李家栋[1]，王昭东[1]，R. D. K. MISRA[2]

1. 东北大学 轧制技术及连轧自动化国家重点实验室，沈阳 110819；
2. Laboratory for Excellence in Advanced Steel Research, Department of Metallurgical, Materials and Biomedical Engineering, University of Texas at El Paso, El Paso, TX 79968, USA

摘 要：采用扫描电镜、透射电镜、拉伸试验及差示扫描量热技术研究不同固溶方式对 Al−Mg−Si 合金组织性能和析出行为的影响。结果表明：热风固溶比电阻固溶的合金再结晶晶粒更加均匀细小。经两种方式固溶后，合金织构不同，电阻固溶产生更多旋转立方织构，有利于提高合金的成形性。冲压前，均匀细小晶粒和基体中大量团簇存在使热风固溶合金强度较高。烤漆时，更多团簇发生转变，同时具有较好的烤硬化性。

关键词：Al−Mg−Si 合金；固溶方式；再结晶晶粒；织构；力学性能；析出激活能

(Edited by Xiang-qun LI)